FOURIER ANALYSIS OF X-RAY MICRODIFFRACTION PROFILES TO CHARACTERIZE LASER SHOCK PEENED METALS

Hongqiang Chen, Y. Lawrence Yao, Jeffrey Kysar, Youneng Wang
Department of Mechanical Engineering
Columbia University, New York, NY 10027

I. Cev Noyan
Thin Film Metallurgy Department, IBM T. J. Watson Research Center
Yorktown Heights, NY 10598

KEYWORDS

Fourier analysis, Microdifraction, Laser shock peening

ABSTRACT

X-ray micro-diffraction profiles using a synchrotron light source were analyzed via Fourier analysis for single crystal Aluminum and Copper samples subjected to micro scale laser shock peening. Specifically, the asymmetric and broadened diffraction profiles registered across the shock peen region were analyzed by the Fourier analysis method. Average strain, mosaic size and dislocation density were extracted for the first time with spatial resolution of 5 μm. The results were compared with the simulation result obtained from FEM analysis and electron backscatter diffraction (EBSD) measurement and good agreements were seen. Difference in response caused by different materials and crystalline orientations was also studied.

INTRODUCTION

Micro-scale laser shock peening (μLSP) is a technique that can improve the fatigue and reliability performances of micro-devices (Zhang and Yao, 2001). Recently, by using the X-ray microdiffraction technology, for the first time, micron level spatial resolution (down to 5μm) of residual stress distribution in the surface of shock peened single crystal Al and Cu was achieved (Chen, et al., 2003a).

In the work of Chen, et al.(2003a), asymmetric and broadened diffraction profiles were observed at each location in the shock peened region, and analyzed by the sub-profiling method and explained in terms of the heterogeneous dislocation cell structure. Residual stress distribution was obtained as a result. To achieve better understanding of microstructure evolution during the process, the spatially distribution of total strain, mosaic size and dislocation density caused by μLSP need to be further studied from the measured X-ray micro-diffraction profile.

Broadening of X-ray diffraction line profiles is often subdivided into size broadening and strain broadening. The classical method to evaluate size and strain broadening using Fourier series coefficients of reflection was developed by Warren & Averbach(1950).

After several attempts to interpret the X-ray line profiles in terms of a microscopic model of materials (Warren and Averbach, 1950; Wilson, 1942; Krivoglaz and Ryaboshapka, 1963), Wilkens (1970) developed a theory for symmet-

rical X-ray diffraction lines broadened by dislocations and dislocation density can be evaluated from the X-ray profile analysis (Ungar and Borbely, 1996).

In this paper, by using classical Warren & Averbach method (1950) and its modification from Ungar (1996), the spatial distribution of strain, mosaic size and dislocation density were evaluated through Fourier analysis of X-ray micro-diffraction profiles for single crystal Al and Cu subjected to μLSP. The result was also compared with other simulation and experimental method such as FEM and EBSD. This analysis directly complements measurements of residual strain/stress in (Chen, et al., 2003a).

EXPERIMENTAL AND SIMULATION CONDITION

Well-annealed single crystals of 99.999% pure Aluminum and Copper were used for micro scale laser shock peening and low order orientations of (110) and (001) are chosen here to achieve high diffraction intensity and study the difference caused by crystal orientation. The Laue diffraction method was used to determine the crystal orientation and the sample was cut to size using a wire EDM.

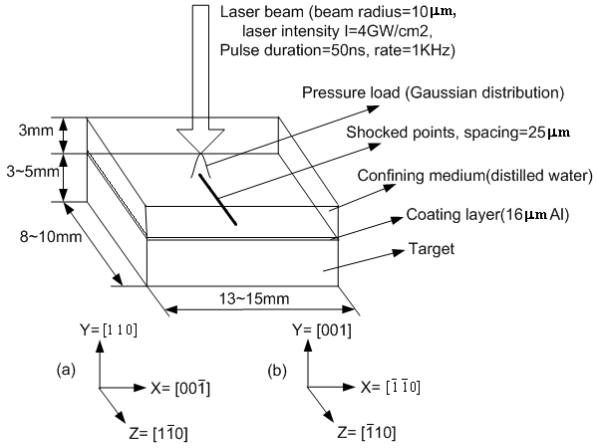

FIGURE 1. SAMPLE GEOMETRY AND LASER SHOCK PEENING CONDITION (DIMENSIONS ARE APPROXIMATE AND MAY VARY SLIGHTLY AMONG SAMPLES).
(A) Al(110) SAMPLE AND Cu(110) SAMPLE
(B) Al (001)SAMPLE

The sample geometry and μLSP setup is shown in Fig. 1. Details of micro-scale LSP setup and sample preparation are referred to (Zhang and Yao, 2000 & 2001; Chen, et al., 2003). In order to understand the overall characteristics of the deformation, the process was also modeled and solved via finite element analysis (FEM). A commercial FEM code, ABAQUS (2002), was used for the simulation. Detail about FEM simulation can be found in the recent paper (Chen, et al., 2003b).

POST-PEENING MATERIAL CHARACTERIZATION

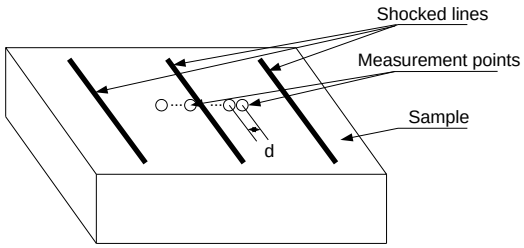

FIGURE 2. X-RAY MICRO-DIFFRACTION MEASUREMENT ARRANGEMENT (MEASUREMENT POINTS ARE ALONG A LINE PERPENDICULAR TO A SHOCKED LINE, MEASUREMENTS WERE CARRIED OUT WITHIN ±100μM FROM THE CENTER OF A SHOCKED LINE, *D*=5μM, WITHIN ±20μM FROM THE SHOCKED LINE CENTER, *D*=10μM, ELSEWHERE).

A high brightness X-ray beam of National Synchrotron Light Source at Brookhaven National Lab was used in diffraction and the beam size was 5 by 7 microns. Multiple measurement points are chosen along a line perpendicular to a shocked line as shown in Fig. 2. At each position, the corresponding X-ray diffraction profile is recorded. For face-centered-cubic (*FCC*) metals, the diffraction structure factor for (110) and (001) are both zero and the reflections are absent (Cullity, 1978). So the (002) and (220) reflections are chosen for (001) and (110) orientation, respectively. For more details of X-ray microdiffraction measurement, please refer to (Chen, et al, 2003a).

In addition to X-ray microdiffraction, electron backscatter diffraction (EBSD) was applied to the shock peened samples. EBSD has some special advantages in microstructure analysis over TEM. The sample preparation of EBSD is not destructive thus the nearly original state of the sample can be observed which is crucial to the shock peening study. A much larger area than TEM can be quantitatively and statistically analyzed. Details about EBSD measurement can be found in (Chen, et al., 2003b).

PRINCIPLES OF FOURIER PROFILE ANALYSIS

X-ray Line Profile Analysis With Warren & Averbach Method

Size Broadening and Strain Broadening. Consider an X-ray profile for reflection (00*l*), since the diffraction profile is the combination of the scattering of X-ray by periodically arranged atoms in the crystal lattice. In the reciprocal space, the X-ray profile can be considered as a Fourier series(Warren, 1969).

Assuming that the diffraction planes in terms of columns of unit cells along the a_3 direction and hence perpendicular to the diffraction planes. The real part of the Fourier coefficients

$$A_n = \frac{N_n}{N_3} < \cos 2\pi l Z_n > \quad (1)$$

Where N_3=average number of cells per column, N_n=average number of *n* pairs per column. $Z_n = n < \varepsilon >$ and $< \varepsilon >$ is the average strain caused by crystal lattice distortion along a3 direction. According the analysis in (Warren, 1969), N_n/N_3 depends only on the column lengths, so it is a size coefficient and we represent it by A_n^S, the other quantity $< \cos 2\pi l Z_n >$ depends on the distortion in the domain represented by A_n^D.

Calculation of Strain Effect and Size Effect. According to Eqn. (1), the real part of coefficient, A_n, which is determined from experiment, is the product of a size coefficient and a distortion coefficient:

$$A_n = A_n^S A_n^D \quad (2)$$

For small values of *l* and *n*, the logarithm of the measured Fourier coefficient is given by:

$$\ln A_n(l) = \ln A_n^S - 2\pi^2 l^2 n^2 < \varepsilon^2 > \quad (3)$$

where ε is the strain.

Dislocation Density Evaluation Using Modified W-A Analysis

From the analysis above, the size effect and strain effect can be obtained by X-ray profile Fourier analysis. However, Warren & Averbach method mentioned above can not recognize the strain broadening caused by dislocations. According the work of Ungar (1996), the analysis of Fourier coefficients have shown that taking into account the contrast caused by dislocations on line profiles gives new scaling factors and can be considered as a modified W-A analysis.

In Ungar's model, for large crystals containing dislocations, the real part of the Fourier coefficients of a peak profile can be written as

$$\ln|A(n)| = c_0 - \rho^* n^2 \ln(R_e / n) + Q^* n^4 \ln(R_2 / n) \ln(R_3 / n) \quad (4)$$

where ρ^* is the "formal" dislocation density, directly available from a broadened profile without taking into account the contrast caused by different types of dislocations. Q^* is related to the two-particle corrections in the dislocation ensemble, which can be given as the fluction of the dislocation density, *n* is the Fourier parameter, and R_e is the outer cutoff radius of dislocations, and R_2 and R_3 are auxiliary constants. The true value of dislocation is

$$\rho = \frac{2\rho^*}{\pi g^2 b^2 \overline{C}} \quad (5)$$

where $\overline{C}$ is the average contrast factor if dislocations in the case of a particular *hkl* reflection and can be found in (Ungar and Borbely, 1996), *b* is the Burgers vector of dislocations which is *a/2*<110> here for *FCC* metals. Eqn.(4) represents a non-linear curve of A_n-*n* with parameters which be determined by curve using least-squares evaluation method. Thus, from the analysis of A_n-*n* curve, the dislocation density ρ can be evaluated.

FOURIER PROFILE ANALYSIS RESULTS

Stoke Correction

To correct for the instrumental broadening in the diffraction pattern of a sample, it is convenient to run a standard peak using a sample in which the particle size is large enough to eliminate all particle-size broadening. *f(y)* is the desired curve which would be obtained if there were no instrumental broadening. *g(z)* is the curve representing instrumental broadening which is obtained from the standard. *h(x)* is the curve from the sample, containing both the desired broadening and the instrumental broadening.

Since the profile from the sample is a convolution of the functions representing particle-size broadening and instrumental broadening. The

Fourier coefficient of the *f(y)*-curve is then given by the simple relation:

$$F(n) = H(n)/G(n) \qquad (6)$$

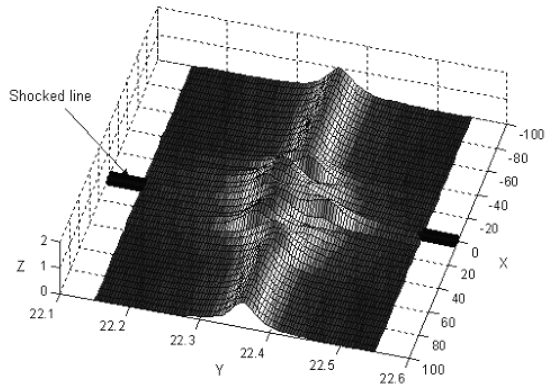

FIGURE 3. 3D X-RAY PROFILE SPATIAL DISTRIBUTION ACROSS THE SHOCKED LINE FOR (002) REFLECTION OF Al (001) SAMPLE (X-AXIS: DISTANCE FROM THE SHOCKED LINE CENTER(μM); Y-AXIS: BRAGG ANGLE(DEGREE); AND Z-AXIS: NORMALIZED DIFFRACTION INTENSITY).

Fig. 3 shows the three dimensional spatial distribution of those measured X-ray profiles for Al (002) reflection. It is clear that after shock peening, the X-ray profile was significantly broadened and became asymmetric compared to unshocked region. Here a typical *h(x)* is the profile measured at the shocked region, the curve *g(z)* is the profile measured at shocked free region. Thus, the corrected X-ray profile *f(y)* is obtained from Eqn. (6).

Average Strain Estimate And Comparison With FEM Simulation

From the theory of Warren and Averbach(1950), for small values of *l* and *n*, the logarithm of the measured Fourier coefficient is given by Eqn. (3) and it represents a straight line with slope $K = -2\pi^2 l^2 < \varepsilon^2 >$. Thus, the average mean square strain from that X-ray profile as:

$$< \varepsilon_l >= \sqrt{\frac{K}{-2\pi^2 l^2}} \qquad (7)$$

In order to obtain the spatial distribution of the average strain, X-ray profiles at each position cross the shocked line were processed using Fourier transformation with Stoke's correction mentioned before. Fourier number n^2 vs the natural logarithm of the real part of the corresponding Fourier coefficient lnA_n for different samples and reflections were shown in Fig. 4. It is clear that the magnitude of line slope increases from the position far away from the shock line center (30μm) to the center of shock line (0μm). The average strain increases gradually when the position moves closer to the shocked center since the magnitude of the slope K is proportional to the average strain. Thus, the average strain in the region close to the shocked line center is larger than that in the region far away from the center.

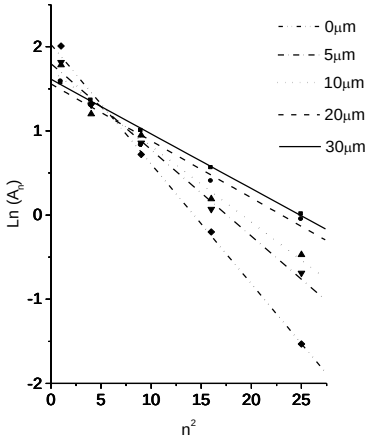

Al (002) reflection

FIGURE 4. Ln(A_N) VS N^2 LINES AT DIFFERENT POSITION FROM THE CENTER OF SHOCKED LINE (A_N: THE REAL PART OF CORRECTED FOURIER COEFFICIENT; AND *N*: FOURIER SERIES NUMBER)

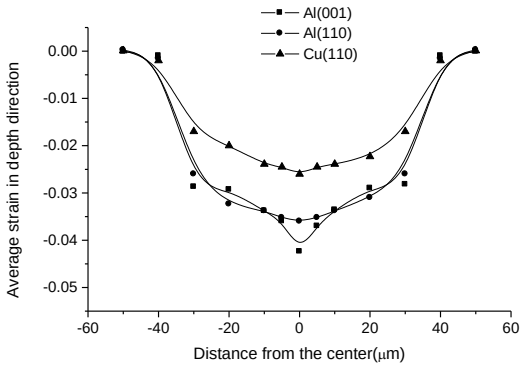

FIGURE 5. SPATIAL DISTRIBUTION OF AVERAGE STRAIN IN DEPTH DIRECTION EVALUATED FROM SLOPE ANALYSIS SHOWN IN Fig. 4

Fig. 5 shows the spatial distribution of calculated average strain value from slope analysis for Al (001), Al (110) and Cu (110) sample shown in Fig. 4. For all samples, the maximum

average strain in depth direction occurs in the shocked line center and decreases with the position away from the center. The region of significant strain is around ±40μm from the center and the magnitude is from -0.043 at the center to near zero when moving away from the center. Also the strain magnitude of Al (110) is significantly larger than that of Cu (110) obviously due to strength difference. However, it is almost identical to that of Al (001) sample and indicates a weak relation of deformation with crystalline orientation under the conditions used.

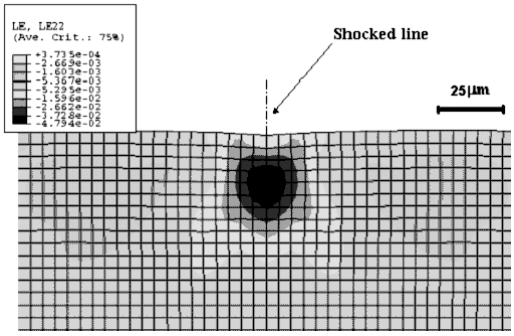

FIGURE 6. TYPICAL FEM SIMULATION RESULT OF STRAIN DISTRIBUTION IN DEPTH DIRECTION, Al (001) SAMPLE: 200×80μM AS SHOWN, TOTAL SIMULATION REGION IS 800×400μM, DEFORMATION FACTOR=5 FOR VIEWING CLARITY

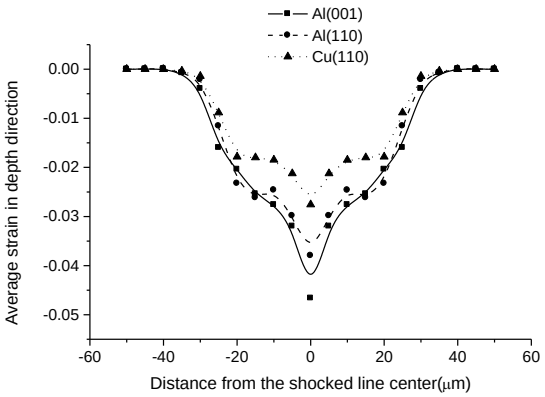

FIGURE 7. SPATIAL DISTRIBUTION OF AVERAGE STRAIN IN DEPTH DIRECTION EVALUATED FROM FEM SIMULATION

To verify the result, FEM simulation was applied to all samples and Fig. 6 shows a typical strain distribution under laser shock peening for Al (001) sample. It is clear that the strain caused by shock peening is compressive and concentrate at the region of about ±25μm from the shocked line center. The maximum strain is around -0.048 and located at depth from 20μm~30μm below the surface. Since the X-ray penetration depth is around 40~50μm here (Cullity, 1978), the strain in depth direction was averaged in this range and compared with the X-ray profile analysis result. Fig. 7 shows the average strain distribution across the shock line region from FEM simulation for all samples. It is clear that the magnitude and the spatial distribution are quite consistent with the result from the FFT profile analysis. Also it can be seen that the strain distribution is almost independent of crystalline orientation but dependent on material difference.

Mosaic Size Estimate And Comparison With EBSD

When a material is deformed, the material is broken into regions with slight tilts with respect to one another and the mosaic size is the size of such small regions. From the analysis of Warren and Averbach(1950), if the measurement of particle size broadening are expressed in terms of a plot of the Fourier coefficients A_n vs n, the initial slope of the curve gives directly the average column length, which is the effective mosaic size in that direction.

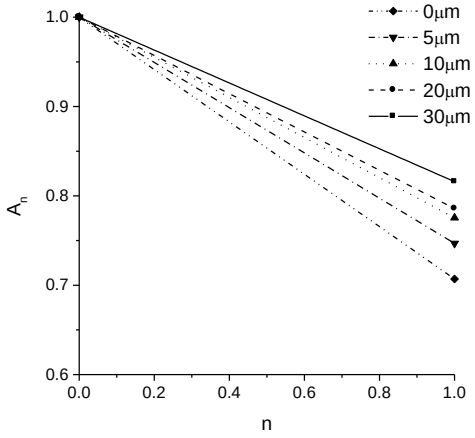

FIGURE 8. THE INITIAL SLOPE OF A_N VS N CURVES FOR Al (001) SAMPLE

For the X-ray profile of (002) reflection for Al (001) sample, Fourier transformation and Stoke's correction were carried out at each positions. Fig. 8 shows the initial slope of those curves (the line connecting the first two points in A_n-n curve) and A_n has been normalized here. If the intercept of these lines with the X-axis is D, and the initial slope of curve is K, then the aver-

age mosaic size *D* at that position can be evaluated as

$$D = (\frac{1}{K}) \cdot a_3 \quad (8)$$

and $$1/2 = (2a_3/\lambda)(\sin\theta - \sin\theta_0) \quad (9)$$

where λ is the wavelength of X-ray, θ is the maximum angle in X-ray profile and θ_0 is the ideal Bragg angle. Using the similar method, the average mosaic size at different positions can be calculated and the spatial distribution can be obtained for all samples.

Fig. 9 shows the spatial distribution of average mosaic size for Al (001), Al (110) and Cu(110) sample evaluated from the X-ray profile analysis mention above. It can be seen that the average mosaic size decreases when the measurement point moves closer to the shock line center for all samples. In the region of ±20μm from the center, the mosaic size is around 1μm to 0.7μm and increases sharply to over 100μm beyond this range. This is reasonable since the shock peening effect is higher in the shock line center and larger plastic deformation will favor the formation of mosaic structure. It is interesting that the results of Al (001) and Al (110) are quite similar, for Cu (110) sample, the average mosaic size is larger than that of Al sample and the submicron mosaic size is limited in the ±10μm region. The overall trend is consistent with the spatial distribution of average strain and the influence of different crystalline orientation is less than different materials.

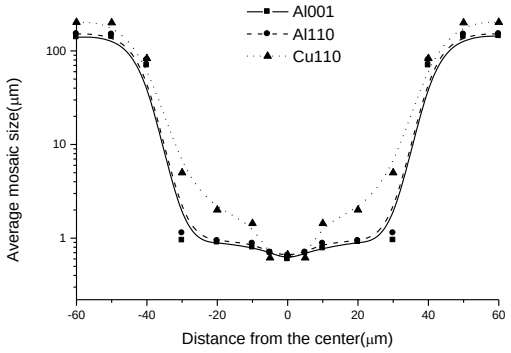

FIGURE 9. SPATIAL DISTRIBUTION OF AVERAGE MOSAIC SIZE FROM INITIAL SLOPE ANALYSIS (Fig. 8)

In addition to using X-ray profile analysis to obtain the mosaic size distribution, EBSD measurement was applied on all samples' surface and mosaic structure was analysis and compared with the result from X-ray. Fig. 10 shows the microstructures of mosaic for Al (110) sample. The thin black lines show mosaic boundaries whose misorientation angles are larger than 3 degrees. The cross sections represented by lines 1,2 and 3 with spacing 12.5μm are made perpendicular to the shocked line. The spatial distribution of mosaic size along the three lines is shown in Fig. 11.

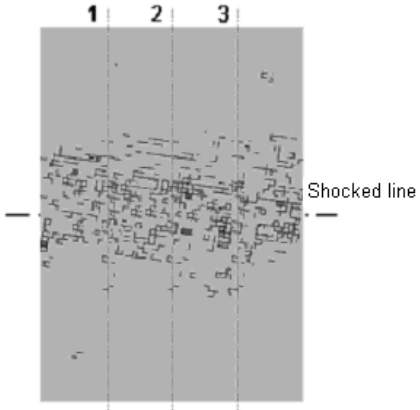

(a)

FIGURE 10. MOSAIC DISTRIBUTION ON SHOCKED PEENED SURFACE MEASURED WITH EBSD (50μM×80μM). THREE CROSS SECTIONS PERPENDICULAR TO THE SHOCKED LINE ARE INDICATED BY 1, 2 AND 3

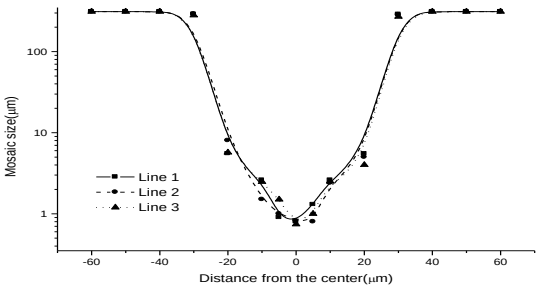

(a) Al (110)

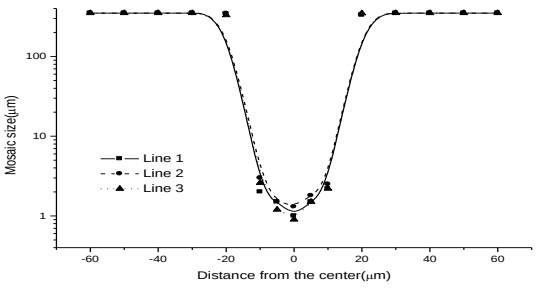

(b) Cu (110)

FIGURE 11. SPATIAL DISTRIBUTION OF MOSAIC SIZE ALONG THE THREE CROSS SECTIONS PERPENDICULAR TO THE SHOCKED LINE

It is observed that within the shock peening region (±20μm from the shock line center for Al

and ±10μm for Cu), it has a larger increase in mosaic structure and the smallest mosaic size(0.8μm for Al and 1μm for Cu) is dominant in the center and become larger away from the shock peened region. The result is consistent with the result obtained from the X-ray profile analysis mentioned before.

The substantial increase of sub-structures is the major cause of strength and hardness improvement in LSP. The formation of mosaic structures has an effect similar to grain refinement. According to Murr(1981), the yield strengths of copper and nickel increase after LSP. Both the compressive surface residual stress and the refined microstructure in LSP contribute to the fatigue life improvement.

Dislocation Density Estimate Using Modified W-A Model

It is of interest to study the magnitude and spatial distribution of dislocation density under μLSP. Within the formalisms of the kinematical scattering of X-rays and the linear elasticity theory of dislocations, modified Warren-Averbach method was used to evaluate the dislocation density from the X-ray profile analysis (Ungar and Borbely, 1996). According to Eqn. (4), nonlinear curve fitting with the least-squares evaluation was applied to the plot of the Fourier coefficients ln(A_n) vs n. All parameters were calculated through curve fitting. After obtaining the formal dislocation density ρ^*, the true values of dislocation density is calculated by Eqn. (5).

Fig. 12 shows the comparison of dislocation density distribution for Al (001), Al (110) and Cu (110) samples. As seen, the highest density occurs at the shock line center and decays slowly to the outer edge. It can be seen that the dislocation structure is most significant in Al (001) sample and less in Al (110) sample, and the least for Cu (110) sample. This can be explained as follows.

The most apparent feature controlling microstructures or microstructure development in *FCC* metals and alloys is the stacking-fault free energy. From the analysis of Chen, et al.(2003a), easy cross slip is an essential mechanism for dislocation formation. In high stacking-fault free energy materials, the stacking fault energy limits the partial dislocations and promotes cross slip of dislocations from one plane to another. So the high stacking-fault will favor the formation of dislocation. Al is the *FCC* metal with the highest stacking-fault free energy (168mJ/m2) and copper is 78mJ/m^2. As a result, the dislocation cell structure can be generated easier in Aluminum than in Copper.

From the analysis of Chen, et al. (2003a) and Stouffer (1996), cross slip is more difficult to occur in the (110) orientation, since there is no common slip direction between different slip planes. However, in (001) orientation, the slip systems $(111)<10\bar{1}>$ and $(\bar{1}1\bar{1})<10\bar{1}>$ can generate the cross slip between these two slip planes. Thus, the cross slip is much easier to occur in (001) orientation than in (110) orientation and this favors the formation of dislocation in (001) orientation.

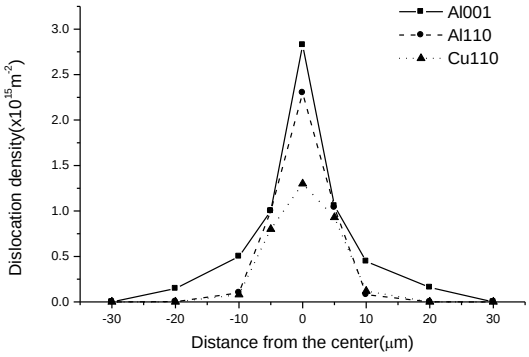

FIGURE 12. SPATIAL DISTRIBUTION OF DISLOCATION DENSITY OBTAINED FROM CURVE FITTING ANALYSIS

CONCLUSIONS

X-ray micro-diffraction profiles analysis using Fourier transformation was realized for single crystal Al and Copper sample subjected to micro scale laser shock peening. The asymmetric and broadened diffraction profiles registered at each location were analyzed by classic Warren & Averbach method (1950) and modified W-A method proposed by Ungar in 1996. Spatial distribution of average strain, particle size and dislocation density were estimated. FEM simulation and EBSD were applied to all samples to verify the result. Micron level spatial resolution (down to 5μm) was achieved. The average strain is around -0.03 to -0.04 within ±30μm from the shocked line center and it decreases to zero beyond that range. The result was found consistent with FEM simulations and more depend-

ent on the different material than different crystalline orientation. Mosaic like substructure was formed in submicron size within the region ±20μm from the shocked line center and consistent with the measurement from EBSD. The asymmetric and broadening profiles are strongly indicative of dislocation formation during LSP and material in (001) orientation and material with higher stack fault energy (Al) shows higher dislocation density under laser shock peening.

ACKNOWLEDGEMENT

This work is supported by the National Science Foundation under grant DMI-02-00334. Dr. Jean Jordan-Sweet of IBM Watson Research Center provided assistance in using the X-ray microdiffraction apparatus at the National Synchrotron Light Source at Brookhaven National Laboratory. Assistance in technical details in sample preparation for EBSD and data analysis by Dr. Yongxue Gang, and Mr. J. B. Chou is also appreciated.

REFERENCES

ABAQUS/Standard User's Manual, (2002), Version 6.2, Hibbit, Karlsson and Sorensen, Inc., Pawtucket, RI, USA.

Chen, H. Q., Y. L., Yao, and J. W., Kysar, (2003a), "Spatially Resolved Characterization of Residual Stress Induced by Micro Scale Laser Shock Peening," *ASME Journal of Manufacturing Science and Engineering*, to appear.

Chen, H. Q., J. W., Kysar, and Y. L. Yao, (2003b), "Characterization of Plastic Deformation Induced by Micro Scale Laser Shock Peening," *ASMEJournal of Applied Mechanics"*, submitted.

Cullity, B. D., (1978), *Elements of X-ray Diffraction*, Addison-Wesley Publishing Company, Inc., London, Second edition, pp. 268-270.

HKL Channel 5TM User's Manuel, (2001), HKL Technology, Danbury, CT.

Krivoglaz, M.A., and K.P., Ryaboshapka, (1963), "Theory of Scattering of X-rays and Thermal Neutrons by Real Crystals", *Fiz. Met. Metalloved.*, Vol.15, pp.18-25.

Murr, L. E., (1981), "Microstructure-Mechanical Property Relations," *Shock-wave and High-Strain-Rate Phenomena in Metals*, Plenum Press, Inc., New York, pp. 607-671.

Stouffer, D.C., and L.T., Dame, (1996), *Inelastic Deformation of Metals*, John Wiley & Sons, Inc., New York, pp. 12-15.

Ungar, T., *et al.*, (1984), "X-ray Line-Broadening Study of the Dislocation Cell Structure in Deformed [001]-Orientated Copper Single Crystals", *Acta metall*., Vol. 32, No. 3, pp. 332-342.

Ungar, T., and A., Borbely, (1996), "The effect of dislocation contrast on x-ray line broadening: A new approach to line profile analysis", *Applied Physics Letter*, Vol. 69, pp. 3173-3175.

Warren, B.E., and B.L., Averbach, (1950), "The Effect of Cold-Work Distortion on X-ray Patterns", *Journal of Applied Physics*, Vol. 21, pp.595-599.

Warren, B.E., (1969), *X-ray Diffraction*, Chap. 13, Addison-Wesley, Reading, MA.

Wilkens, M., (1970). *In Fundamental Aspects of Dislocation Theory, Natl Bur. Stand. (US) Spec. Publ.* No. 317. Washington, DC, USA.

Wilson, A. J. C., (1942), "Imperfections in the Structures of Cobalt. II. Mathematical Treatment of Proposed Structure", *Proc. R. Soc. London Ser. A,* Vol. 180, pp. 277-285.

Zhang, W. W. and Y. L., Yao, (2001), "Feasibility Study of Inducing Desirable Residual Stress Distribution in Laser Micromachining," *Transactions of the North American Manufacturing Research Institution of SME* (*NAMRC XXIX) 2001,* pp. 413-420.

Zhang, W. W. and Y. L., Yao, (2000), "Micro Scale Laser Shock Processing of Metallic Components," *ASME Journal of Manufacturing Science and Engineering*, Vol. 124, No. 2, pp. 369-378.